ORIGINAL RESEARCH ARTICLE

Graphite–WS_2 Copper-Based Self-lubricating Composites Prepared by Spark Plasma Sintering

YONGDU LI, YUAN ZHANG, YANG LI, XIAOHONG WANG, JUNJIE HUANG, and MEI YANG

In this study, nickel-plated graphite/WS_2 copper matrix composites with varying contents were prepared using the spark plasma sintering (SPS) technique. The porosity, mechanical properties, and tribological properties of these composites were investigated. The results indicate that increasing the mass ratio of WS_2 to nickel-coated graphite results in higher porosity and lower compressive strength of the composites. The increase in hardness suggests that porosity has a significant effect on compressive strength, and the formation of Cu_2S at the Cu–WS_2 contact site is the primary reason for this increase. Among the composites, the Cu–20Gr–10WS_2 composite exhibits the lowest friction coefficient (0.21) and wear rate (3.35×10^{-5} mm^3/nm). This composite also shows a well-developed self-lubricating film and a smooth wear surface. The XPS etching reveals a lubricant film thickness of approximately 14.5 nm, and the main wear mechanism observed is adhesive wear.

https://doi.org/10.1007/s11661-023-07212-8

I. INTRODUCTION

METAL-BASED self-lubricating composites are highly valued in the field of tribology because of their exceptional properties.[1–4] These composites are prepared through powder metallurgy and comprise a metal matrix material combined with a solid lubricant. The metal matrix materials commonly used are Fe, Al, Cu, and Ni, among others, while the solid lubricants include graphite, MoS_2, WS_2, graphene, and more.[5–8]

In recent years, copper-based graphite composites have been extensively employed in self-lubricating friction parts, such as brushes and contact rods, in various industries including mechanical transmission, transport, military, and aerospace. This is primarily due to their exceptional mechanical strength, excellent thermal conductivity, and self-lubricating properties.[9–12] However, the solubility between copper and graphite is low because of their differences in chemical properties and crystal structure.[13–15] Despite attempts to improve this through treatment, the resulting composites have low mechanical properties (hardness), leading to a decrease in their lubrication properties.[16–18] When the hardness of a composite material decreases, its surface becomes more susceptible to scratching and abrasion, leading to damage and loss of lubricant. This diminishes the presence of lubricant on the friction surface, thereby reducing lubrication effectiveness. Furthermore, the decreased hardness can cause an increase in the surface roughness of the composite material, which in turn elevates friction and frictional heat, further diminishing lubrication effectiveness. Simultaneously, reduced hardness may induce deformation and plastic changes in the material. Under high loads and high friction conditions, the material may experience plastic deformation, consequently impacting lubricant distribution and lubrication effectiveness. In addition, with increasingly harsh service conditions, traditional copper-based graphite composites can no longer meet the current needs. Therefore, it is necessary to seek a solid lubricant that can form a strong interfacial bond with the copper matrix and provide effective lubrication like graphite. Some researchers have found WS_2 with self-lubricating properties that can replace graphite. It has been found that WS_2 with too little participation cannot exert good self-lubricating properties, while WS_2 with a large amount of participation has excellent self-lubricating properties, but too much WS_2 will lead to an increase in the porosity of the composites, which seriously affects their mechanical properties and thus reduces their wear-resistant properties.[6,19–21] Studies have shown that the combination of two or more solid lubricants can achieve a good synergistic lubrication effect, and its performance is

YONGDU LI is with the School of New Energy and Materials, Southwest Petroleum University, Chengdu 610500, P.R. China. YUAN ZHANG and YANG LI are with the Sichuan Petroleum Construction Co. Ltd, Chengdu 610213, P.R. China. XIAOHONG WANG, JUNJIE HUANG, and MEI YANG are with the School of New Energy and Materials, Southwest Petroleum University. Contact e-mail: 380056676@qq.com.
Manuscript submitted July 18, 2023; accepted September 20, 2023.
Article published online October 11, 2023

better than that of a single lubricant.[22,23] In the past decades, there have been many reports on improving the lubrication performance of copper matrix graphite composites. Li *et al.*[24] and Gardos *et al.*[25] discussed the synergistic lubrication mechanism of copper-based graphite and MoS_2, and the results of the study showed that there is a good synergistic lubrication effect between graphite and MoS_2, which can significantly improve the wear resistance of epoxy composites. Although MoS_2 can maintain its lubricity at a high temperature of 1000 °C, it has been found that the addition of MoS_2 reduces the hardness of the composite and increases the plasticity which will affect its friction properties.[26] Jiang[27] discussed the synergistic lubrication mechanism of copper-based graphite and PTFE and found that the copper-based graphite sample impregnated with PTFE had better wear resistance. However, the intolerance of PTFE material to high temperatures limits its application. WS_2 has excellent load-bearing capacity, high-temperature resistance, wider temperature adaptability, longer lubrication life, lower coefficient of friction, and graphite-like laminate structure, making it an effective solid lubricant alternative to PTFE and MoS_2.[6,20] Copper-based graphite/WS_2 composites are widely utilized in various applications across microelectronics, aerospace, and mechanical drive industries, primarily because of their exceptional mechanical, physical, and self-lubricating properties. These applications encompass thermal management components boasting excellent thermophysical and mechanical characteristics,[28] high-performance aerospace brushes,[29] as well as mechanical self-lubricating parts designed for low-speed operating conditions.[30] Unfortunately, there are very limited studies on the co-lubrication of copper-based graphite-WS_2 self-lubricating composites. Therefore, an in-depth study of the co-lubrication mechanism of copper-based graphite-WS_2 self-lubricating composites is important for a better understanding and application of the composites.

In this study, copper-based self-lubricating composites containing different contents of nickel-coated graphite and WS_2 were prepared using discharge plasma sintering (SPS). Dry friction wear experiments were carried out under atmospheric conditions to investigate the effect of content on their tribological behavior. By studying the friction morphology change and microstructure, the wear mechanism is explored and the evolution of the friction surface properties is revealed, with a view to providing a theoretical basis for the engineering application of Cu-based graphite-WS_2 self-lubricating composites.

II. MATERIALS AND METHODS

A. *Raw Materials and Material Preparation*

Figure 1 demonstrates the scanning electron microscope (SEM) images of the feedstock powders. Figures 1(a) through (c) shows SEM images of the base material spherical copper powder (99.5 pct purity, < 300 mesh), self-lubricating solid phase nickel-coated graphite powder (Ni75C25, < 300 mesh), and WS_2 powder (99.9 pct purity, < 300 mesh), respectively. These powders were purchased from Tianjin Yiborui Chemical Co. in China.

To avoid a large number of chemical reactions between WS_2 and Cu matrix, spark plasma sintering (SPS) was chosen to prepare the samples in this experiment because it has the characteristics of rapid heating and sintering, which can reduce the reaction between Cu and WS_2 to some extent.[21,31] The process for preparing the copper-based composite material by SPS is shown in Figure 2, and the main process comprises the steps of weighing, grinding, vacuum drying, and SPS sintering. First, according to the composition of the composites, we take the corresponding raw material powders in the following proportions: Cu–30 wt pct nickel-coated graphite (Cu–30Gr), Cu–30 wt pct tungsten disulfide (Cu–30WS_2), Cu–25 wt pct nickel-coated graphite−5 wt pct tungsten disulfide (Cu–25Gr–5WS_2), Cu–20 wt pct nickel-coated graphite−10 wt pct tungsten disulfide (Cu–20Gr–10WS_2), and Cu–15 wt pct nickel-coated graphite−15 wt pct tungsten disulfide (Cu–15Gr–15WS_2). To ensure that the copper-based self-lubricating composites contain intact nickel-coated graphite particles, the team chose a lower percentage of ball-to-powder ratio to avoid the nickel-coated graphite from being over-abraded during the ball milling process. The weighed ingredients were homogeneously mixed in a ball milling tank for 10 h with a mass ratio of ball-milled pellets to powder of 2:1. Next, the milled powder was dried in a vacuum oven at 120 °C for 5 h. Finally, the mixed powder was sintered by hot pressing under the protection of a pure nitrogen atmosphere at 40 MPa at a sintering temperature of 800 °C for a duration of 10 min. A round cake-like specimen with a diameter of 40 mm was finally obtained.

B. *Analysis of Phase Composition, Microstructure, and Mechanical Properties*

The pie-shaped specimens were processed by wire-cutting to meet specific dimensional requirements, and their microstructural, mechanical, and tribological properties were investigated. The size of the samples used for the microstructure, hardness, and tribological tests was 10 mm × 10 mm × 5 mm, and the compression test sample was a cylinder with a diameter of 6 mm and height of 9 mm. The density and porosity of the composites were tested following Archimedes' principle from the literature.[19] According to the requirements of national standard GB-9097.1-88, the HBE-3000A Brinell hardness tester was used to test the Brinell hardness of the specimen. The experimental parameters were set as HBS2.5/62.5 using a hardened steel ball with a diameter of 2.5 mm as the indenter, an experimental force of 62.5 kgf, and a holding time of 30 s. Ten points were tested on samples with different composition contents, and the average value was taken as the hardness value of the copper matrix composites with that content. Compression tests were carried out using a universal material testing machine (SHT4605) with a

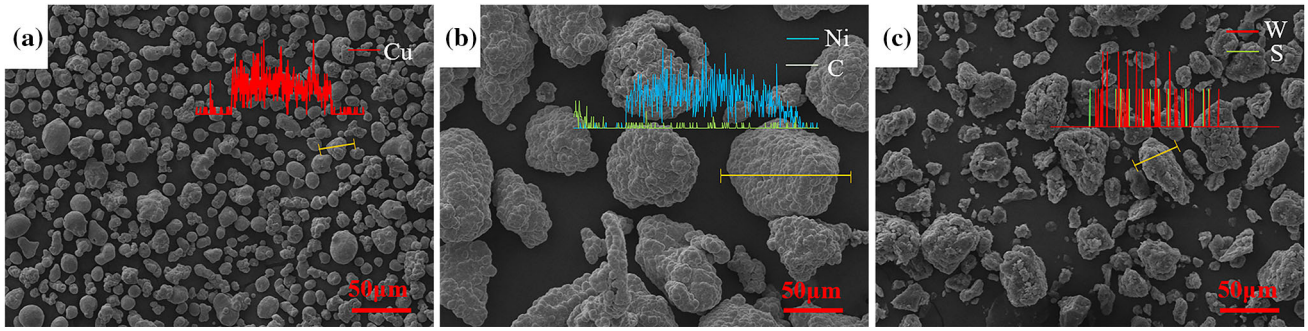

Fig. 1—SEM image of the raw powder.

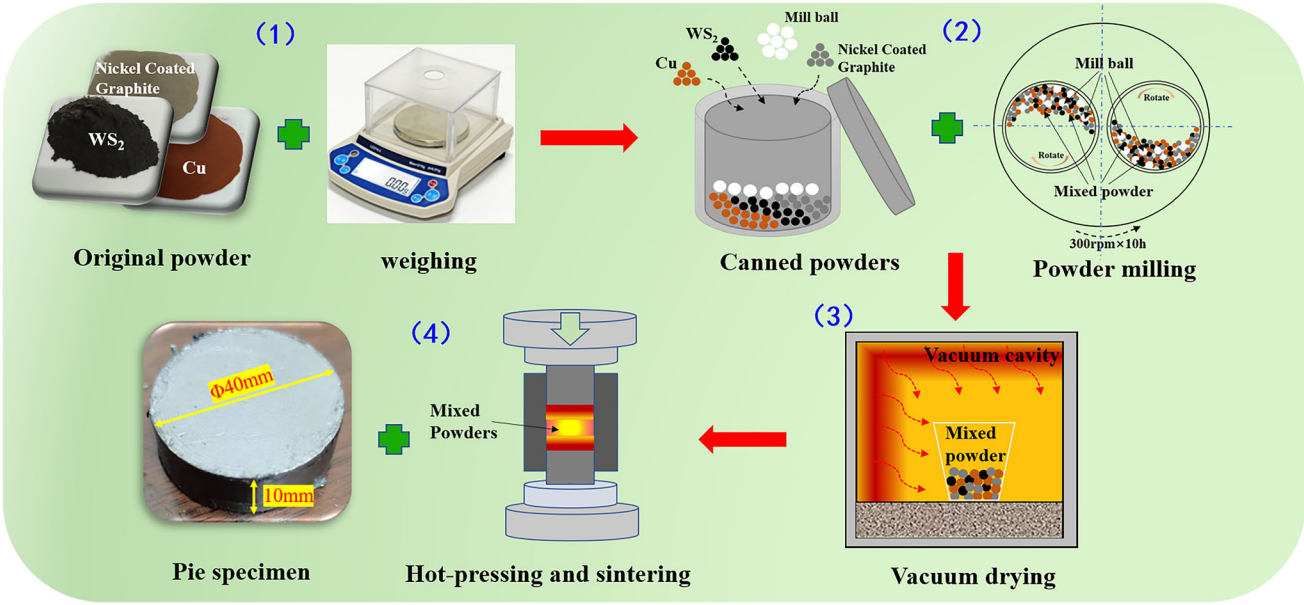

Fig. 2—Process flow chart of composite material preparation.

constant speed of 0.5 mm/min for each content. Three compression tests were carried out for each content of composite material.

The physical characterization of the composites was carried out using an x-ray diffractometer (X'pert pro) using Cu-Kα radiation from 10 to 80 deg at a scanning rate of 10°/min. To better calibrate the graphite material, the characteristic peaks of graphite were detected in the experiments with an in situ variable-temperature, high-pressure laser confocal microscopic Raman spectrometer of the LabRam HR Evolution model, using a blue light incident at 473 nm. A scanning electron microscope (SEM, ZEISS EVO/MA15) equipped with energy-dispersive x-ray spectroscopy (EDS) was used to carry out micro-observations of microstructures, compression sections, and wear surfaces of the composites. The thickness of the lubricated films was analyzed by x-ray photoelectron spectroscopy (XPS, Thermo Scientific K-Alpha), which was equipped with an Al-K alpha-ray excitation source (1486.6 eV) and operated in constant analyzer energy mode, using energies of 100 and 50 eV for measurements and high-resolution spectra, respectively. Ar + ions with an energy of 3 keV were used for etching to measure the distribution of elements at depth, with an etching area size of 1 × 1 mm^2 and etching rate of about 0.29 nm/s. XPS measurements were carried out at cumulative etch times of 0, 15, 30, 50, 100, 200, and 300 s.

C. *Dry Friction and Wear Experiment*

Friction and wear experiments were carried out on a reciprocating ball-on-flat tribometer (UMT-TRIBOLAB). A bearing steel (GCr15) pellets with a diameter of 5 mm and hardness of 62-65HRC was used as the counterpart. The normal load is 20 N, which corresponds to an initial maximum Hertzian contact compressive stress of 432.44 MPa. Sliding wear tests were conducted under normal laboratory conditions (50 to 60 pct relative humidity at 25 to 30 °C), and the friction test parameters are shown in Table I. Prior to the friction experiments, the composite surfaces were polished using 500, 800, 1200, 2000, and 3000 grit sandpaper; finally, the specimens were ultrasonically cleaned using anhydrous ethanol. The cross-sectional area of the wear marks (mm^2) was obtained by white light

Table I. Friction test parameters

Speed (mm/s)	Time (min)	Scratch Distance (mm)	Sliding Load (N)
5	20	5	20

interferometry, and the wear volume was obtained by multiplying the cross-sectional area by the one-way scratch length. However, this calculation may slightly overestimate the friction rate because of the parabolic shape of the observed wear scars. The wear rate (mm^3/nm) was evaluated by the formula[32]:

$$W = \frac{V}{f \cdot L}$$

where W is the wear rate, V is the wear volume (mm^3), f is the friction force (N), and L is the single-pass friction distance (mm). Three parallel tests were performed on the wear rate at each load.

III. RESULTS AND DISCUSSION

A. *Microstructure and Phase Analysis*

Figure 3 illustrates the physical phase characterization of the copper-based self-lubricating composite. Panel a shows the X-ray diffraction (XRD) pattern of the composite. In the composite containing 30 pct nickel-coated graphite, only the diffraction peaks of the copper substrate can be observed, and there are no apparent graphite diffraction peaks. This is attributed to the encapsulation of graphite in nickel, which makes the direct detection of graphite diffraction peaks challenging. To more accurately confirm the presence of the graphite phase, graphite in the composites was examined using Raman spectroscopy. As depicted in Figure 3(b), there are three characteristic peaks in the Raman spectrum appearing at 1350 cm^{-1}, 1590 cm^{-1}, and 2700 cm^{-1}, corresponding to the D, G, and 2D peaks of graphite, respectively. The D peak signifies the incompleteness and disorder in the structure of the graphitic material, while the G peak arises from the stretching vibration of the C-C bond, indicating the completeness and order in the structure of the graphitic material. Additionally, no new phases were detected in the composites containing 30 pct nickel-coated graphite. The composite material containing 30 pct WS_2 not only has the diffraction peaks of Cu and WS_2 but also finds a new diffraction peak with a weak peak at the position of 45.79 deg. Through the comparison of the PDF card, this peak belongs to the diffraction peak of Cu_2S, which indicates that part of Cu reacts with WS_2 to form Cu_2S during SPS sintering, with the corresponding chemical reaction formula[33]:

$$4Cu + WS_2 = 2Cu_2S + W$$

No new diffraction peaks were found in the composites of Cu–25Gr–5WS_2 and Cu–20Gr–10WS_2 except the corresponding diffraction peaks of the substrate. The diffraction peaks of the Cu–15Gr–15WS_2 composite were similar to those of the substrate, and a weak Cu_2S diffraction peak was also found at the position of 45.79 deg. Notably, when the content of WS_2 is higher, the presence of Cu_2S can be detected in the composites, but the measured Cu_2S diffraction peaks are very weak, which indicates that the reaction between Cu and WS_2 can be controlled at a lower level by SPS sintering technology.

The uniform distribution of solid lubricant ensures uniform distribution of lubricant film on the wear surface, which in turn affects the tribological properties of self-lubricating composites to some extent.[34] Figure 4 shows the microscopic results of the prepared copper-based self-lubricating composites, which include SEM images. The SEM image in Figure 4(a) shows that the black nickel-coated graphite is uniformly distributed in the copper matrix when the copper matrix contains 30 wt pct nickel-coated graphite and no obvious defects such as pores are found, indicating that the composites are structurally dense under this process. Figure 4(b) illustrates the SEM image of the copper matrix containing 30 wt pct of WS_2. The white WS_2 particles are distributed relatively uniformly, and small amounts of gray phases present in the image. Most of these gray phases are found surrounding the white WS_2 particles.

EDS elemental analysis confirms that these gray phases primarily consist of S and Cu elements, with an atomic ratio close to 1:2. Based on the XRD results, it can be inferred that the gray phase corresponds to Cu_2S, which forms because of the reaction between S and Cu at high temperatures. Notably, there are also black flocculent distributions at the grain boundaries of the matrix copper. By EDS analysis, the Cu element becomes a concave trend, and W and S elements are not detected, which can be presumed to belong to the pore space, consistent with the results of Zhao *et al.*[21] The SEM maps of Figures 4(c) through (d) show the uniform distribution of Ni-coated graphite and WS_2. Notably, the gray phase Cu_2S in the composite gradually increases with the increase of WS_2 content, while the pores in the composite increase, leading to the disruption of the continuity of the copper matrix.

The evolution of the interfacial structure of composites has a significant impact on their mechanical properties.[35–37] The characterization of the composite interfaces, as shown in Figures 4(f) and (g), reveals the formation of a black phase at the interface between the Cu matrix and WS_2 in Figure 4(f). EDS analysis results in Figure 4(b) confirm that this black phase is a Cu_2S compound formed by the reaction between copper and WS_2 at elevated temperatures. Cu_2S acts as a binder at the interface, effectively bonding the copper matrix and WS_2 particles together. However, due to the poor compatibility between copper and WS_2, the Cu_2S layer is unable to completely fill the voids in the material, resulting in the presence of pores between the Cu_2S layer and the copper matrix, consequently leading to a lower density of the composite. On the other hand, as depicted in Figure 4(g), no discernible pores or defects are observed in the micromorphological map of the

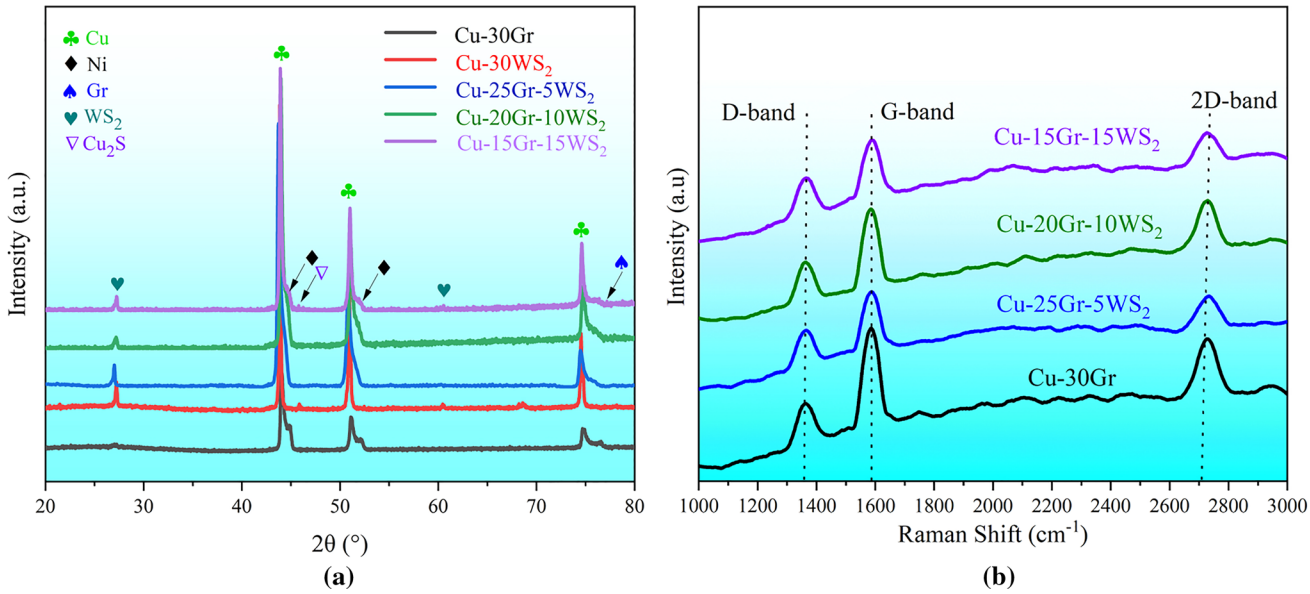

Fig. 3—(*a*) XRD pattern of copper-based self-lubricating composite material; (*b*) Raman spectroscopy of graphite in composites.

interface between nickel-coated graphite and copper matrix. This indicates that the use of nickel-coated graphite can effectively reduce the porosity of the graphite phase in the composites and overcome the challenge of achieving dense sintering of graphite during the powder metallurgical process. Consequently, nickel-coated graphite not only reduces the porosity of the composites but also contributes to enhancing their density.

Porosity is an inherent characteristic of powder metallurgy materials, which affects the mechanical, physical, chemical, and technological properties of materials to a certain extent.[38] The density and porosity of copper-based self-lubricating composite

materials are illustrated in Figure 5. The porosity of Cu–30Gr and Cu–30WS_2 composites is measured at 2.3 and 5.6 pct, respectively. These results indicate that, under identical processing conditions, the Cu–30Gr composite displays a higher density, whereas the Cu–30WS_2 composite exhibits a lower density. These findings align with the earlier SEM results discussed. The high density of the Cu–30Gr composite can be attributed to the nickel plating on the surface of the graphite. This is because the nickel on the graphite surface forms a solid solution with the matrix copper, resulting in an infinite mutual solubility. Additionally, at high temperatures, graphite can dissolve in the lattice of nickel in the form of monomeric carbon. This transformation changes the interfacial bonding of the composite from a simple mechanical interlocking bond to a solid solution bond with gradient changes.[39] The lower densification of the Cu–30WS_2 composite is attributed to the inability of the matrix Cu to intercalate with WS. Instead, only a thin layer of the compound Cu_2S is formed at the Cu/WS_2 interface (as seen in the SEM image, gray Cu_2S is distributed around WS_2). When Ni-coated graphite and WS_2 are blended, the porosity of the composite material gradually increases as the mass ratio of WS_2 to Ni-coated graphite increases. The Cu–15Gr–15WS_2 composite demonstrates the highest porosity, reaching a value of 5.1 pct. This observed trend in porosity variation aligns with the changes observed in the SEM images and is in line with the reported results in the literature.[6]

B. *Mechanical Properties of Composites*

The hardness of the self-lubricating composites is depicted in Figure 6. The Cu–30Gr and Cu–30WS_2 composites exhibit Brinell hardness values of 172 HB and 260 HB, respectively. This indicates that composites containing WS_2 have higher hardness when the mass of the solid lubricant is kept constant. The hardness of the copper-based self-lubricating composites increases with the higher mass ratio of WS_2 and nickel-coated graphite when the two solid lubricants are mixed. The Cu–15Gr–15WS_2 composite displays the highest hardness value of 215 HB. It is generally believed that the porosity of a material exhibits the same trend as its hardness. However, based on the above results, the porosity has a lesser effect on the hardness of Cu matrix composites when Ni-encapsulated graphite and WS_2 are co-mingled. The main reason for this hardness trend can be explained from two perspectives. First, as the WS_2 content increases, WS_2 and the Cu matrix react to form Cu_2S at high temperatures, thereby enhancing the interfacial bond strength between WS_2 and the Cu matrix.[40] Second, this trend can also be attributed to the anisotropic properties of WS_2.[41]

The compressive strength of the copper-based self-lubricating composites is depicted in Figure 7. The compressive strengths of Cu–30Gr and Cu–30WS_2 composites are 131 MPa and 66 MPa, respectively. This demonstrates that composites containing nickel-coated graphite exhibit higher compressive strengths while keeping the mass of the solid lubricant constant. When

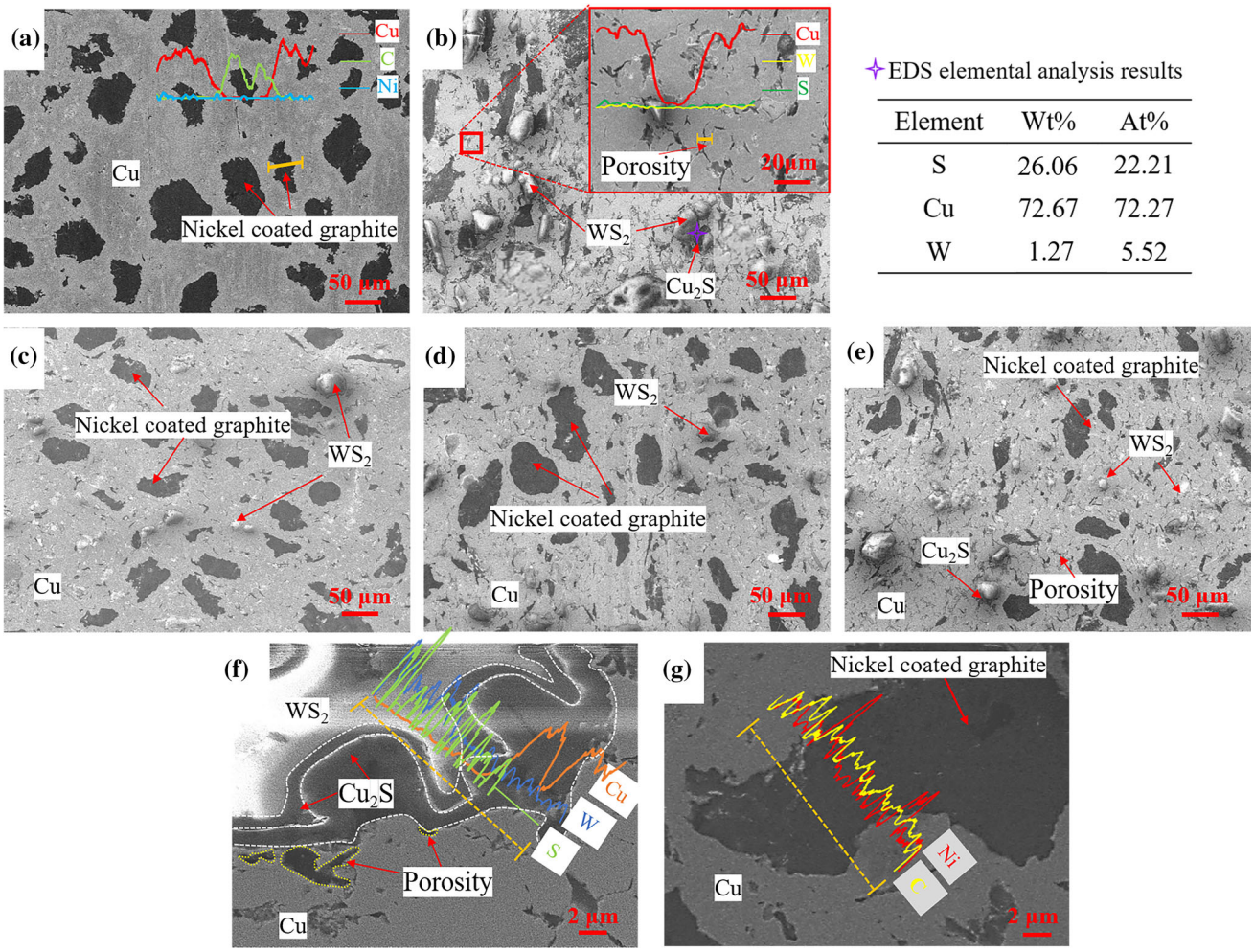

Fig. 4—SEM micrographs of the microstructure of the composite: (*a*) Cu–30Gr; (*b*) Cu–30WS_2; (*c*) Cu–25Gr–5WS_2; (*d*) Cu–20Gr–10WS_2; (*e*) Cu–15Gr–15WS_2. (*f*) The interface between copper and WS_2 in composites; (*g*) the interface between copper and nickel-coated graphite in composites.

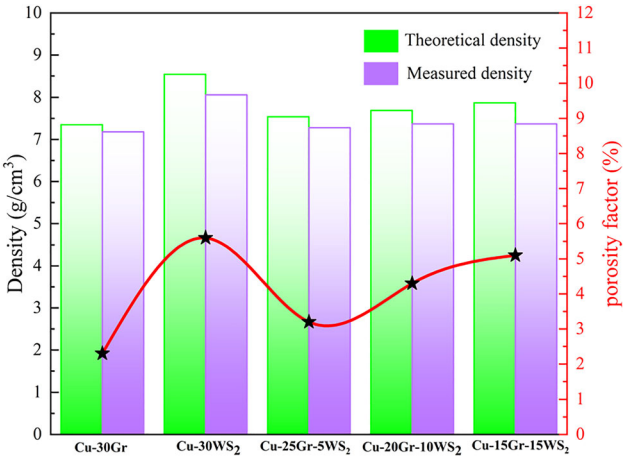

Fig. 5—Density and porosity of copper-based self-lubricating composites.

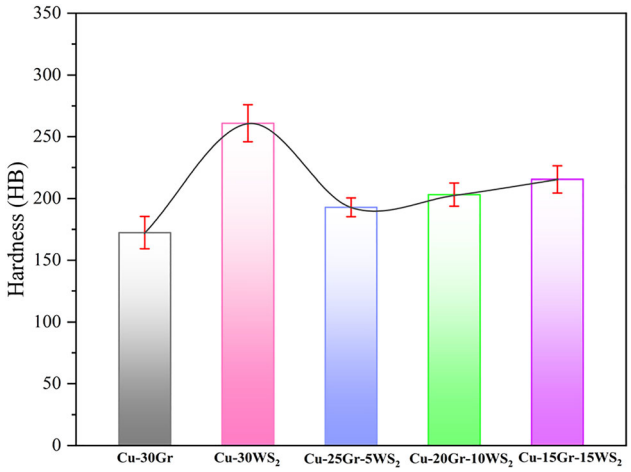

Fig. 6—Hardness values of copper-based self-lubricating composites.

the two solid lubricants are mixed, the compressive strength of the copper-based self-lubricating composites decreases with an increase in the mass ratio of WS_2 and nickel-coated graphite. The Cu–25Gr–5WS_2 composite exhibits the highest compressive strength value of 123 MPa.

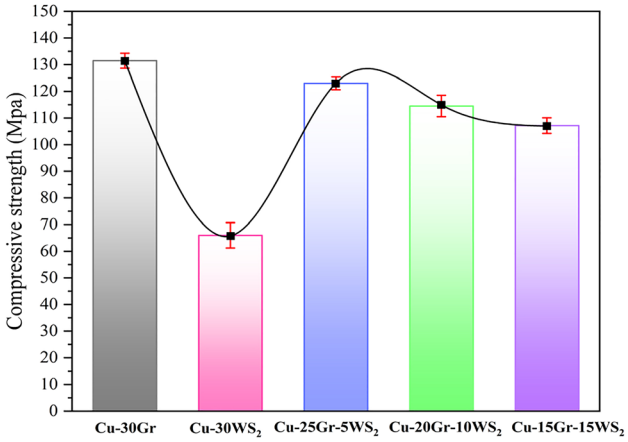

Fig. 7—Compressive strength values of copper-based self-lubricating composites.

To gain a deeper understanding of the fracture mechanism of copper-based self-lubricating composites, the compressive fractures of the composites were analyzed microscopically using a scanning electron microscope, and their micro-morphology is presented in Figure 8. First, it is important to emphasize that under the same experimental conditions, the Cu–70Gr and Cu–25Gr–5WS_2 composites did not fracture but rather exhibited a significant amount of plastic deformation. This indicates that copper can still maintain its excellent plastic deformation ability even when incorporating a certain amount of nickel-coated graphite, which also offers a better explanation for the higher compressive strength observed in Figure 7 for these two composites. As Figure 8(a) shows, the fracture of the composite containing only 30 pct WS_2 appears relatively smooth, with minimal plastic deformation of the material. The type of fracture is characteristic of brittle fracture. The fracture also exhibits numerous cracks, with evident crack extension. Micro-mechanism analysis (Figures 4(b) and 5) reveals that the primary cause of the aforementioned brittle fracture is the high WS_2 content, resulting in the formation of numerous pores within the composite material. As depicted in Figure 8(b), no cracks were observed on the fracture surface of the Cu–20Gr–10WS_2 material. Instead, a significant number of tough nests were present, indicating substantial plastic deformation of the material. The fracture surface appeared relatively rough, suggesting a plastic fracture type. As depicted in Figure 8(c), the fracture surface of the Cu–15Gr–15WS_2 material exhibits both cracks and tough nests. Additionally, some plastic deformation is evident in the material, indicating a combination of plastic and brittle fracture.

C. *Friction and Wear Properties of Composites*

Figure 9 illustrates the coefficient of friction for copper-based self-lubricating composites. As depicted in Figure 9(a), when the copper matrix contains only 30 pct of nickel-coated graphite, the friction coefficient is high and exhibits instability. However, when the same mass of nickel-coated graphite is replaced with WS_2, the friction efficient of the composite is significantly reduced, and the curve becomes more stable. This phenomenon can be attributed to the fact that WS_2 is more prone to forming a favorable self-lubricating film on the friction surface under the same horizontal load, thereby creating separation between the friction partners and reducing the coefficient of friction. Studies have shown that intact self-lubricating films can reduce the coefficient of friction.[34,42] Additionally, the Cu–30WS_2 composite possesses higher hardness, which further contributes to a lower coefficient of friction. When the two solid lubricants are combined, the friction coefficient curves of the composites exhibit marked differences compared to those of the Cu–30Gr but closely resemble those of the Cu–30WS_2. Figure 9(b) presents the average friction coefficient of the copper-based self-lubricating composites. It is evident that the average coefficient of friction for the Cu–30Gr composite is 0.4, approximately twice that of the Cu–30WS_2. Significantly, the average coefficient of friction for the composites shows an initial decrease followed by an increase as the mass ratio of WS_2 and nickel-coated graphite increases. The Cu–20Gr–10WS_2 composite demonstrates the lowest average coefficient of friction at 0.12. This finding suggests that the optimal synergistic lubrication effect is attained with a ratio of 20 pct nickel-coated graphite and 10 pct WS_2.

After conducting the friction test, the wear rate can be determined by analyzing the depth and width of the wear track on the composite material. The wear track morphology of the copper-based self-lubricating composites is illustrated in Figure 10. As depicted in Figures 10(a) and (b), the wear track depth of the Cu-30Gr composite measures approximately 1145 μm, and its width is around 30 μm. In contrast, the wear track depth of the Cu–30WS_2 composite is approximately 455 μm, with a width of about 8 μm. The significant reduction in depth and width suggests that WS_2 can effectively decrease the friction loss rate of Cu-based composites with the same mass compared to an equivalent mass of nickel-clad graphite. When the two solid lubricants are combined, the depth and width of the wear tracks in the composites tend to initially decrease and then increase with the increasing mass ratio of WS_2 to nickel-coated graphite. Among these composites, the Cu–20Gr–10WS_2 exhibits the smallest depth and width of wear tracks, measuring 424 μm and 6 μm, respectively.

Based on the statistics and calculations, the friction rate of the copper-based self-lubricating composites is illustrated in Figure 11. From the figure, it is evident that the composite with only 30 pct Ni-coated graphite exhibits the highest friction loss rate of 10.58×10^{-5} mm^3/nm, followed by Cu–30WS_2. Notably, the friction loss rates of the composites blended with both solid lubricants are lower than that of a single solid lubricant, indicating a synergistic lubrication effect between the Ni-coated graphite and WS_2. Among the two solid lubricant blends, Cu–20Gr–10WS_2 shows the lowest friction loss rate of 3.35×10^{-5} mm^3/nm. Previous studies have shown a close relationship between the friction loss rate of composites and the coverage degree

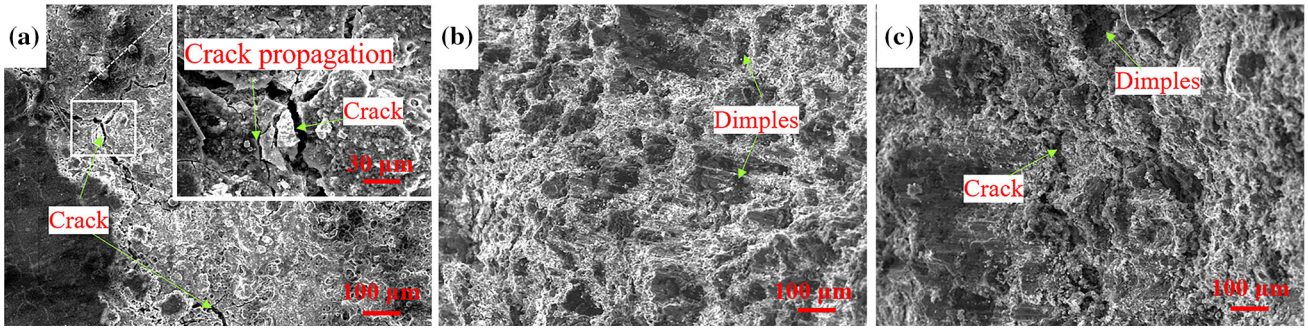

Fig. 8—Morphology of compression section of copper-based self-lubricating composite: (*a*) Cu–30WS_2; (*b*) Cu–20Gr–10WS_2; (*c*) Cu–15Gr–15WS_2.

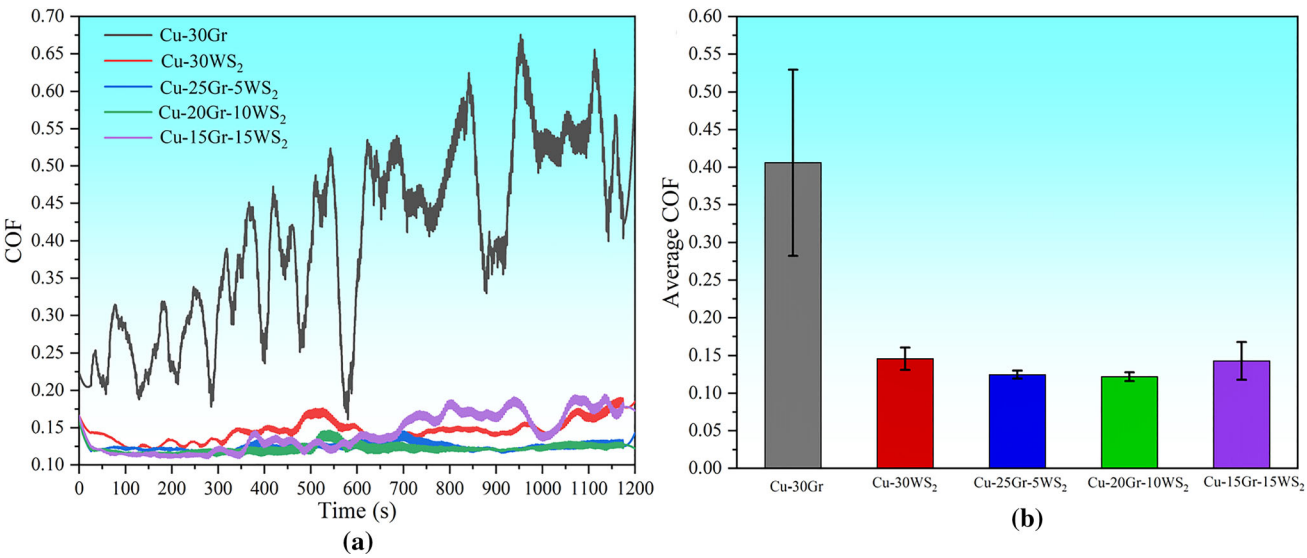

Fig. 9—Friction coefficient of Cu-based self-lubricating composite. (*a*) Friction coefficient curve, (*b*) average friction coefficient.

of the self-lubricating film on the friction surfaces, where a higher coverage degree typically results in a lower friction loss rate.[43–45] The lowest friction loss rate of Cu–20Gr–10WS_2 may be because 20 pct Gr and 10 pct WS_2 form the most complete self-lubricating film during friction. When the content of WS_2 is increased to 15 pct, the friction loss rate increases, mainly because too much WS_2 leads to a large number of pores and cracks in the composites, which is detrimental to the mechanical properties of the composites and therefore should be avoided as much as possible.[46] This conclusion is consistent with the previous findings on porosity and compressive section cracking.

D. *Analysis of Wearing Surface and Self-lubricating Film*

Figure 12 shows SEM images of the wear surface of the copper-based self-lubricating composite. The wear surface of the composite containing only 30 pct nickel-coated graphite (Figure 12(a)) shows the presence of grooves, friction debris, and adhesion pits as well as a thin film on the wear track. A large amount of nickel-coated graphite remained intact, indicating that a large amount of graphite self-lubricating film was not formed during friction, but rather a metallic film dominated. The wear surface is rougher, providing a better explanation for why the Cu–30Gr composite exhibits the highest friction rate. The formation of grooves can be attributed to the plowing effect caused by the harder bumps and wear debris in the friction pair on the softer copper matrix. The friction process generates a significant amount of heat, leading to the formation of adhesion pits on the wear surfaces due to repeated squeezing. Furthermore, oxidation occurs on the wear surfaces exposed to the atmosphere, as the friction takes place under atmospheric conditions. Similar phenomena have been observed in numerous other Cu-based composites.[47,48] This indicates that the primary wear mechanisms of Cu–30Gr composites are adhesive wear and oxidative wear. Compared to Cu–30Gr, the wear surface of Cu–30WS_2 composites shows no noticeable grooves or adhesion pits, and the film thickness on the wear track is significantly greater than that of Cu–30Gr. Hence, the wear mechanism of Cu–30WS_2 is adhesive wear, albeit to a lesser degree.

As depicted in Figures 12(c) through (e), when the two solid lubricants are combined, the coverage degree of the

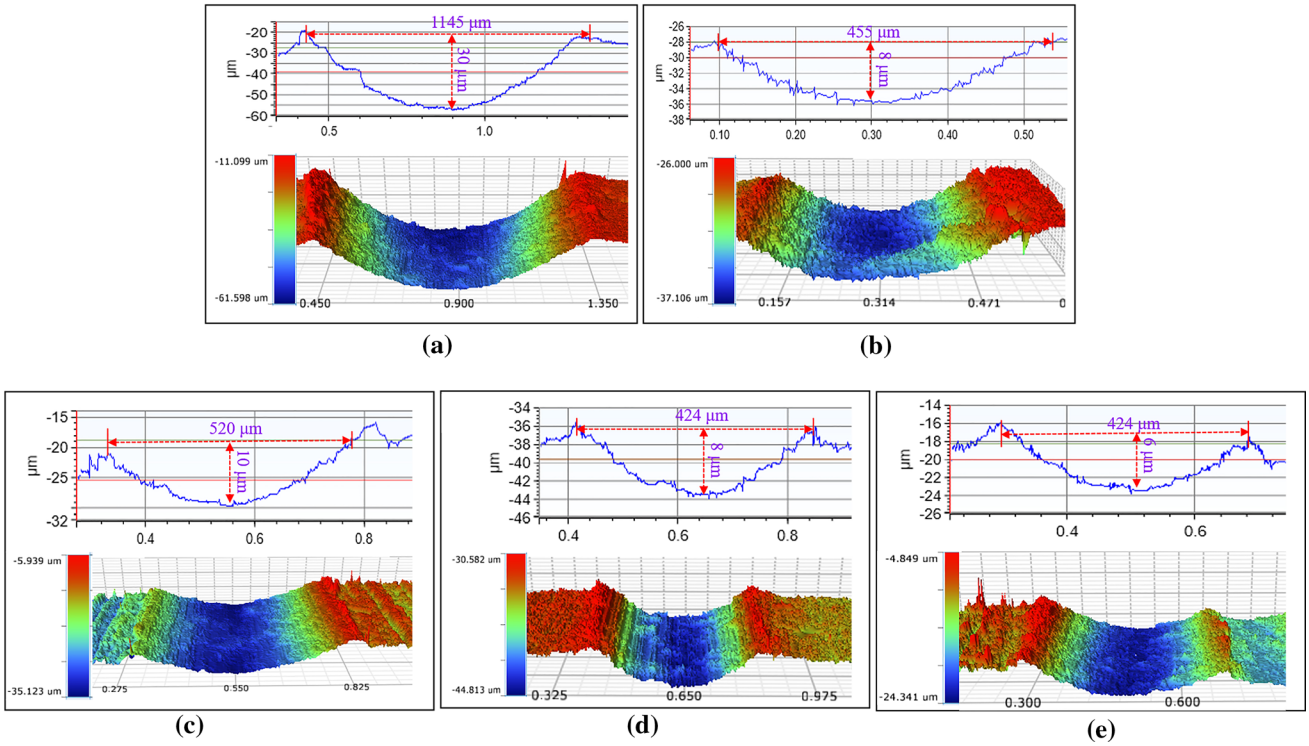

Fig. 10—Wear trace morphology of Cu-based self-lubricating composite: (*a*) Cu–30Gr; (*b*) Cu–30WS_2; (*c*) Cu-25Gr-5WS_2; (*d*) Cu-20Gr-10WS_2; (*e*) Cu–15Gr–15WS_2.

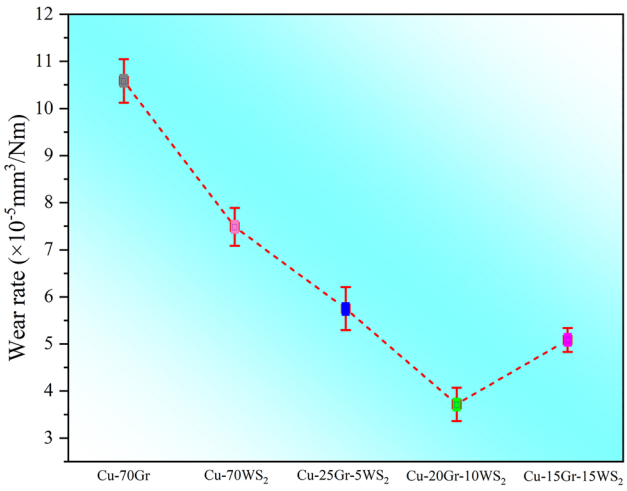

Fig. 11—Wear rate of copper-based self-lubricating composite material.

self-lubricating film on the wear surface of the composites gradually increases with the increase in the mass ratio of WS_2 and nickel-coated graphite (the coverage degree of Cu–20Gr–10WS_2 and Cu–15Gr–15WS_2 is approximately the same). Additionally, the wear surface becomes smoother, and the corresponding oxidative and adhesive wear mechanisms are significantly reduced. Although the Cu–15Gr–15WS_2 composites form a relatively complete self-lubricating film, the wear rate is higher compared to Cu–20Gr–10WS_2. This is primarily attributed to excessive WS_2 disrupting the continuity of the Cu matrix, resulting in many pores and reduced mechanical properties. The Cu–20Gr–10WS_2 composite exhibits the most complete formation of a self-lubricating film on the wear surface, which holds significant research value. Figure 12(f) provides a magnified view of Figure 12(d), revealing a substantial amount of fine debris present within the gaps of the self-lubricating film. Comparing the EDS elemental analysis of point 1 (fine debris) and point 2 (lubrication film) indicates that the fine debris represents the refined lubrication film. Similar fine debris was also found in Cu–25Gr–5WS_2 and Cu–15Gr–15WS_2 composites with relatively low lubricating film coverage. This fine debris serves to fill the cracks, pits, and broken sections of the worn surface, effectively replenishing and enhancing the smoothness of the lubrication film. Consequently, a favorable lubrication effect can be achieved.[49] Under high loads, the formation of fine debris occurs as the instantaneous transfer of frictional heat is hindered, leading to elevated temperatures that soften the material. Moreover, the impact and shear forces between the concave and convex features on the opposing friction surfaces become sufficiently strong to cut through the micro-convexities. Consequently, the micro-convexities within the lubrication film are sheared and crushed. This phenomenon has also been observed by Bin *et al.* in C/SiC wear experiments with varying loads.[50,51] At higher loads, the fine debris present within the C/SiC lubrication film fills the surface defects, thereby demonstrating its advantageous role in improving the lubrication properties.[52]

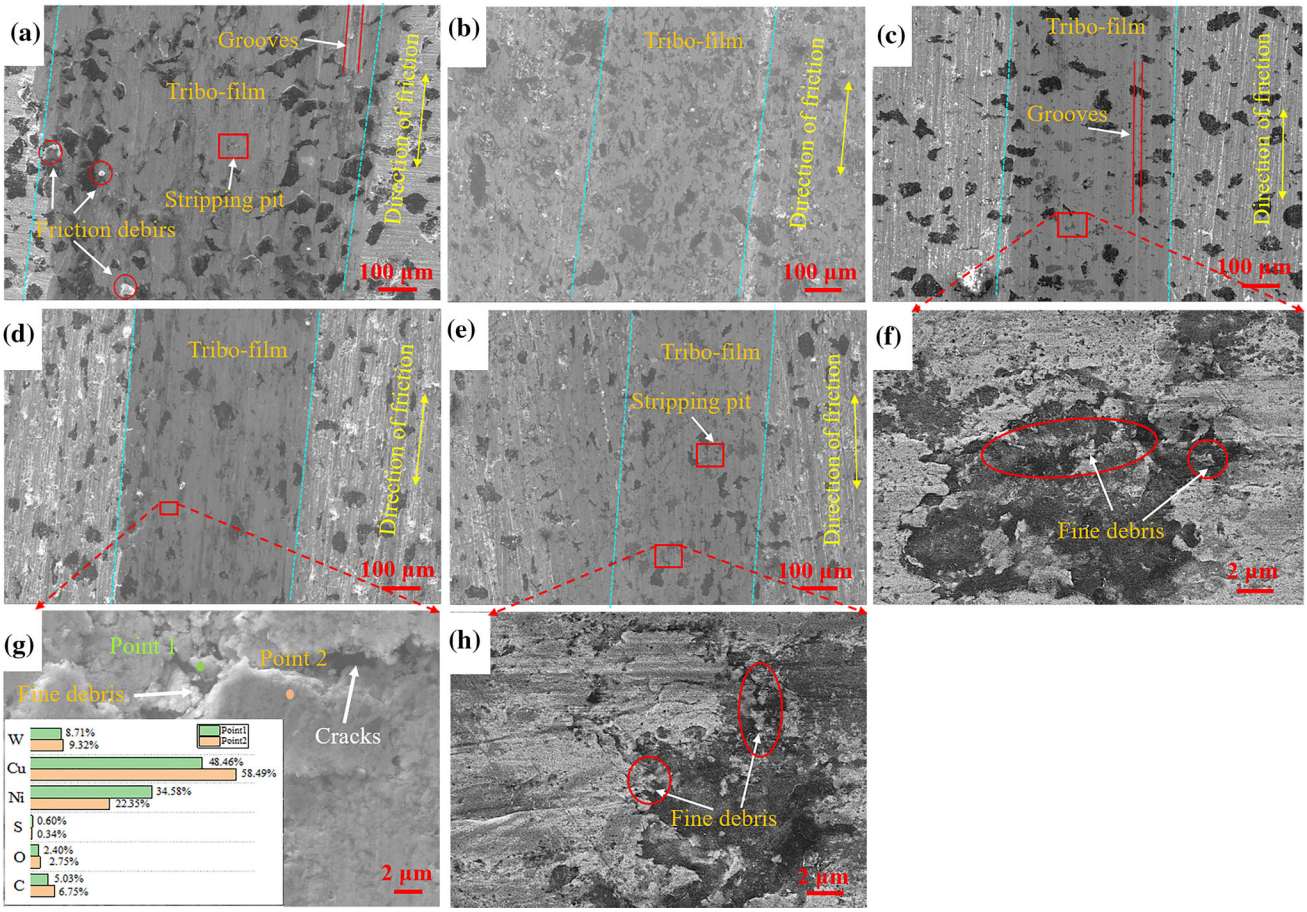

Fig. 12—SEM images of the worn surfaces of Cu-based self-lubricating composites: (*a*) Cu–30Gr; (*b*) Cu–30WS_2; (*c*) Cu–25Gr–5WS_2; (*d*) Cu–20Gr–10WS_2; (*e*) Cu–15Gr–15WS_2. (*f*) Enlarged view of figure c; (*g*) enlarged view of figure d; (*h*) enlarged view of figure.

Figure 13 presents the results of the EDS energy spectroscopy analysis conducted on the wear surface of the Cu–20Gr–10WS_2 composite. Through an examination of the elemental distribution of graphite and WS_2, both possessing self-lubricating properties, it was discovered that carbon (C), tungsten (W), and sulfur (S) elements were uniformly distributed across the wear surface. Therefore, it can be inferred that during the friction process, WS_2 and graphite were extracted from the copper matrix and evenly deposited onto the wear surface. After multiple reciprocating frictions, a thin self-lubricating film was formed. This self-lubricating film effectively contributed to the reduction of wear.

Based on the aforementioned analyses, it can be concluded that the Cu–20Gr–10WS_2 composite exhibits a low coefficient of friction and the lowest rate of friction loss. The self-lubricating film formed on the friction surface is exceptionally smooth and intact, thereby rendering it of significant research value. To investigate the thickness and composition of the friction film, XPS etching was employed to characterize the wear trajectory of the Cu–20Gr–10WS_2 composite. The etching process utilized an ion beam size of 400 μm within the time range of 0–100 s. Figure 14(a) illustrates that the intensities of the Cu2p peaks were measured as 932.5 and 952.3 eV, respectively, with the depth and Cu content in the vertical direction increasing as the Ar + ion etching time progressed. Figures 14(b) and (c) demonstrates that the spectra of O1s and C1s exhibit an inverse trend to that of Cu2p, as the content of O1s and C1s gradually diminishes with increasing etching time. Notably, the relatively elevated levels of oxygen and carbon at 0 s are primarily attributed to the adsorption of atmospheric oxygen and carbon pollutants on the friction surface, resulting in a relatively lower content of other elements. Figures 14(d) and (e) presents the XPS spectral patterns of S2p and W4s, which display similar but not identical trends, suggesting that the composition of the lubricating film on the friction surface is not solely comprised of C and WS_2, and a small amount of Cu_2S formed may be formed. Figure 14(f) illustrates the depth distribution trend on the friction wear surface of the Cu–20Gr–10WS_2 composite. It was observed that prior to etching, the content of other elements remained low because of the presence of surface-adsorbed oxygen and carbon contamination (with carbon already exceeding 20 pct). Following etching, the content of other elements gradually increased as the surface-adsorbed oxygen and carbon contamination were removed. After 30 of etching, the content of nickel, carbon, sulfur, and tungsten elements experienced a rapid decrease. Beyond 50 of etching, the

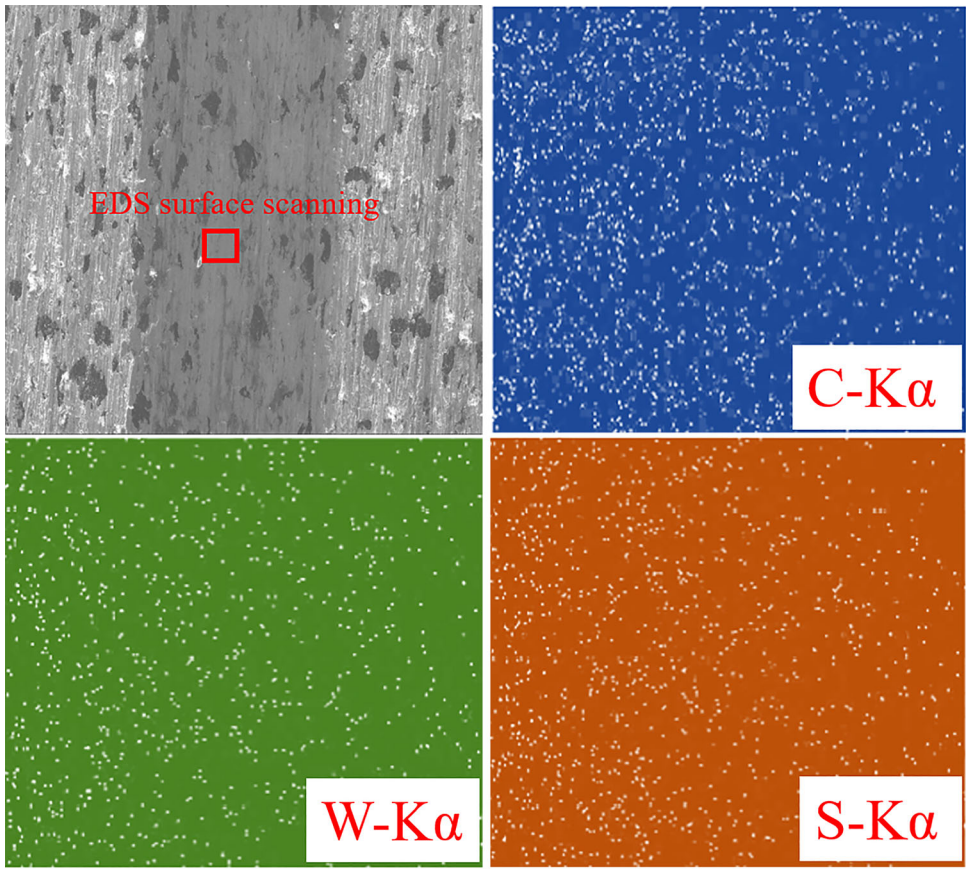

Fig. 13—EDS analysis results of worn surface of Cu–20Gr–10WS_2 composite.

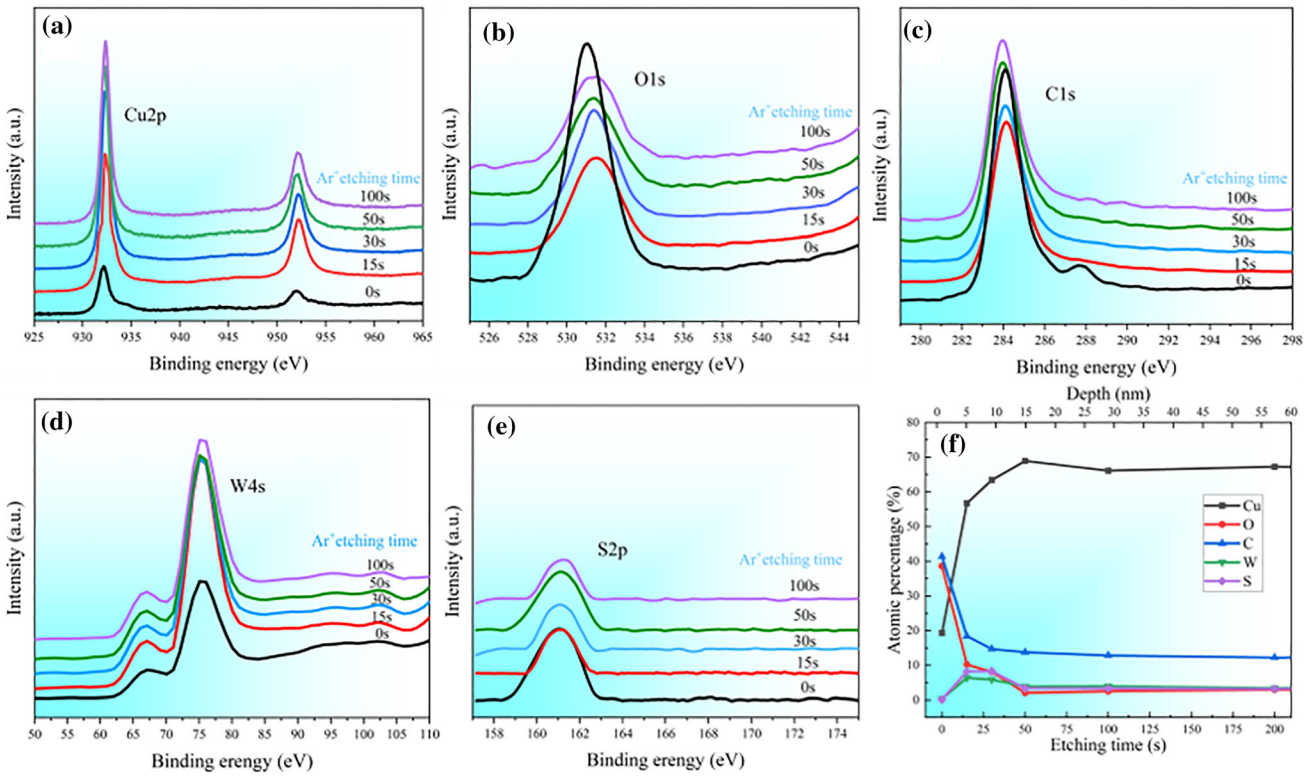

Fig. 14—XPS spectra as a function of etching time on the worn surface of Cu–20Gr–10WS_2 composite.

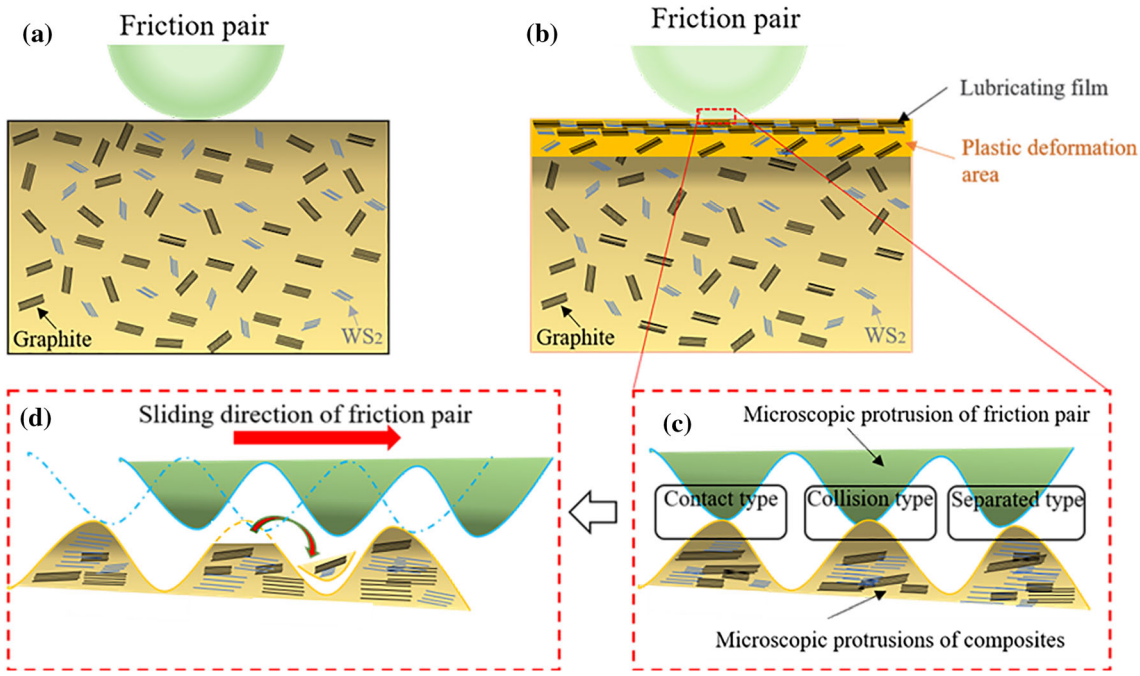

Fig. 15—Schematic diagram of wear mechanism of Cu–Gr–WS_2 composite: (*a*) before friction; (*b*) after friction; (*c*) before micro-protrusion collision friction; (*d*) after micro-protrusion collision friction.

content of carbon, sulfur, and tungsten elements reached a stable state, indicating the etching removal of the self-lubricating film containing carbon, sulfur, and tungsten, with the total content of nickel, carbon, sulfur, and tungsten being approximately equivalent to the amounts of graphite and WS_2 added to the material. Considering the XPS etching rate of 0.29 nm/s, it can be estimated that the thickness of the self-lubricating film in the Cu–20Gr–10WS_2 composite is approximately 14.5 nm.

E. *Wear Mechanism Analysis*

Based on the above analyses, a wear mechanism model for Cu-based graphite–WS_2 composites is proposed, as illustrated in Figure 15. Graphite and WS_2, which possess self-lubricating properties, are randomly distributed within the copper matrix (Figure 15(a)). After the reciprocal sliding of the friction pair, the composite surface undergoes severe plastic deformation. The WS_2 in the plastic deformation region exhibits a high level of orientation after sliding because of the combined effect of the plastic mobility of the Cu matrix and the high stiffness of Cu_2S formed between WS_2 and Cu. Moreover, graphite within the subsurface cavity of the Cu matrix easily deforms along with the subsurface matrix.[53] During sliding friction, the graphite is extruded onto the wear surface and mechanically mixed with WS_2 and other fragmented particles between the contacting surfaces. Subsequently, it is coated by shear stresses on the friction surface, resulting in the formation of a solid lubrication film composed of a mixture of graphite and WS_2 (Figure 15(b)).

The friction wear surface of Cu–20Gr–10WS_2 composites is very smooth and forms a complete self-lubricating film, which can be explained by the theory of frictional microprojectile contact and collision.[54] The friction wear behavior is mainly caused by the contact and collision of micro-protrusions between the friction partner and the material being rubbed. According to the friction theory, when the deformation of two micro-protrusions in contact with each other exceeds their own elastic limit, the micro-protrusion with lower hardness will be the first to undergo plastic deformation. The contact collision model of micro-protrusions is established, as shown in Figures 15(c) and (d). Even if on the surface of the smooth friction ball and the composite material surface microscopically there are defects in the tiny protrusions when the friction ball and the composite material are in contact with each other, there are three ways of existence between the tiny protrusions, namely, tiny protrusion contact, tiny protrusion collision, and tiny protrusion separation type. When the relatively hard friction ball slides through, the micro-protrusions on the softer lubrication film will be cut off by the micro-protrusions of the friction ball under a larger cutting force, and these cut-off fine debris of the lubrication film will fill in the broken lubrication film pits (Figure 15(d)). By repeating this process, the broken lubrication film is replenished, resulting in a very smooth friction surface with the lowest coefficient of friction of the Cu–20Gr–10WS_2 composite. Similarly, in the frictional wear of Cu–20Gr–10WS_2 and Cu–20Gr–10WS_2 composites, there is a large amount of fine debris replenishment of the broken lubrication film.

IV. CONCLUSIONS

Copper-based self-lubricating composites were prepared by SPS technology, and the microstructure, mechanical, and tribological properties of the composites with different contents were studied. The conclusions are as follows:

1. The porosity of the Cu–30WS_2 composite is 5.6 pct, which is 2.4 times that of the Cu–30Gr composite. With the increase of the mass ratio of WS_2 to nickel-coated graphite, the porosity of the composites increases gradually, which leads to the decrease of the compressive strength.
2. The Brinell hardness of Cu–30Gr composite is 260 HB and that of Cu–30WS_2 composite is 172 HB. The Brinell hardness of the composites increases with the increase of the mass ratio of WS_2 to nickel-coated graphite.
3. Cu–20Gr–10WS_2 composite exhibits excellent synergistic lubrication performance, with a friction coefficient as low as 0.12 and a corresponding wear rate as low as 3.5×10^{-5} mm^3/nm. With the increase of the mass ratio of WS_2 to nickel-coated graphite, the wear type changes from oxidation wear and adhesive wear to adhesive wear, and the degree of adhesive wear decreases.

ACKNOWLEDGMENTS

This research work was supported by the Natural Science Foundation of Sichuan Province of China (2022NSFSC0325), Application foundation project of Sichuan Science and Technology department (no. 2021YJ0346) and State Key Laboratory of Long-life High-Temperature Materials (DTCC28EE200795).

AUTHOR CONTRIBUTIONS

YL: Data curation, Writing—original draft preparation; YZ: Software; YL: Supervision; XW: Software, Validation; JH: Writing—review and editing; MY: Conceptualization, Methodology.

DATA AVAILABILITY

All data and models generated or used during the study appear in the submitted article.

COMPETING INTEREST

The authors declare no competing interests.

REFERENCES

1. J. Cheng, F. Li, S. Zhu, J. Hao, J. Yang, W. Li, and W. Liu: *J. Wear*, 2017, vol. 386–387, pp. 39–48.
2. M. Grandin and U. Wiklund: *J. Wear*, 2018, vol. 398–399, pp. 227–35.
3. K. Rajkumar and S. Aravindan: *J. Tribol. Lett*., 2010, vol. 37, pp. 131–39.
4. J. Zhen, J. Cheng, S. Zhu, J. Hao, Z. Qiao, J. Yang, and W. Liu: *J. Tribol. Int*., 2017, vol. 110, pp. 52–56.
5. M.M.H. Bastwros, A.M.K. Esawi, and A. Wifi: *J. Wear*, 2013, vol. 307, pp. 164–73.
6. S. Huang, Y. Feng, H. Liu, K. Ding, and G. Qian: *J. Mater. Sci. Eng.: A*, 2013, vol. 560, pp. 685–92.
7. H. Tan, S. Wang, Y. Yu, J. Cheng, S. Zhu, Z. Qiao, and J. Yang: *J. Tribol. Int*., 2018, vol. 122, pp. 228–35.
8. L. Zhang, J. Xiao, and K. Zhou: *J. Tribol. Trans*., 2012, vol. 55, pp. 473–80.
9. W. Chen, P. Feng, L. Dong, M. Ahangarkani, S. Ren, and Y. Fu: *J. Surf. Coat Tech*., 2018, vol. 353, pp. 300–08.
10. K.H. Cho, U.S. Hong, K.S. Lee, and H. Jang: *J. Tribol. Lett*., 2007, vol. 27, pp. 301–06.
11. C. Ma, G.Q. He, D.H. He, C.S. Chen, and Z.F. Hu: *J. Wear*, 2008, vol. 265, pp. 1087–92.
12. X.U. Wei, H.U. Rui, J. Li, Y. Zhang, and H. Fu: *J. Trans. Nonferr. Met. Soc. China*, 2012, vol. 22, pp. 78–84.
13. H. Kato, M. Takama, Y. Iwai, K. Washida, and Y. Sasaki: *J. Wear*, 2003, vol. 255, pp. 573–78.
14. J. Kováčik, Š Emmer, J. Bielek, and L. Keleši: *J. Wear*, 2008, vol. 265, pp. 417–21.
15. S.F. Moustafa, S.A. El-Badry, A.M. Sanad, and B. Kieback: *J. Wear*, 2002, vol. 253, pp. 699–710.
16. R. Voitovitch, A. Mortensen, F. Hodaj, and N. Eustathopoulos: *J. Acta Mater*., 1999, vol. 47, pp. 1117–28.
17. L. Yang, P. Shen, Q. Lin, F. Qiu, and Q. Jiang: *J. Mater. Chem. Phys*., 2010, vol. 124, pp. 499–503.
18. L. Yang, P. Shen, Q. Lin, F. Qiu, and Q. Jiang: *J. Appl. Surf. Sci*., 2011, vol. 257, pp. 6276–81.
19. H. Cao, Z. Qian, L. Zhang, J. Xiao, and K. Zhou: *J. Tribol. Trans*., 2014, vol. 57, pp. 1037–43.
20. R. Tyagi, R. Tyagi, A.K. Das, and A. Mandal: *J. Tribol. Int*., 2018, vol. 120, pp. 80–92.
21. L. Zhao, P. Yao, T. Gong, H. Zhou, M. Deng, Z. Wang, Z. Zhang, Y. Xiao, and F. Luo: *J. Tribol. Lett*., 2019, vol. 67, p. 98.
22. J.L. Li and D.S. Xiong: *J. Wear*, 2008, vol. 265, pp. 533–39.
23. G. Xian, R. Walter, and F. Haupert: *J. Appl. Polym. Sci*., 2006, vol. 102, pp. 2391–2400.
24. X. Li, Y. Gao, J. Xing, Y. Wang, and L. Fang: *J. Wear*, 2004, vol. 257, pp. 279–83.
25. Q. Wang, X. Zhang, and X. Pei: *J. J MACROMOL SCI B*, 2010, vol. 50, pp. 213–24.
26. X. Liang, P. Wu, L. Lan, Y. Wang, Y. Ning, Y, Wang, and Y. Qin: *J/OL. Materials*, 2023, vol. 16.
27. D. Jiang, Z. Jiang, J. Zhang, P. Lin, B. Peng, H. Zhang, J. Liao, W. Li, and J. Zou: *J. ChemistrySelect*, 2020, vol. 5, pp. 14331–39.
28. X. Wang, Y. Su, Q. Ouyang, and D. Zhang: *J. Alloys Compd*., 2022, vol. 916, p. 165318.
29. N. Hiraoka: *J. Wear*, 2001, vol. 249, pp. 1014–20.
30. Shuang-Ding C S-Y X R-R L C-S Z: J. Northeastern Univ., 2007, vol. 9, pp. 1285–88.
31. Z.A. Munir and M. Ohyanagi: *J. Mater. Sci*., 2021, vol. 56, pp. 1–5.
32. X. Liu, X. Shi, G. Lu, X. Deng, H. Zhou, Z. Yan, Y. Chen, and B. Xue: *J. Alloys Compd*., 2019, vol. 777, pp. 271–84.
33. Y. Liang, Y. Che: J. Northeast University Press, 1993.
34. J.-K. Xiao, W. Zhang, L.-M. Liu, L. Zhang, and C. Zhang: *J. Wear*, 2017, vol. 384–385, pp. 61–71.
35. Y. Xie, X. Meng, Y. Chang, D. Mao, Z. Qin, L. Wan, and Y. Huang: *J. Adv. Sci*., 2022, vol. 9, p. 2104464.
36. Y. Xie, X. Meng, Y. Chang, D. Mao, Y. Yang, Y. Xu, L. Wan, and Y. Huang: *J. Compos. Sci. Technol*., 2022, vol. 219, p. 109225.
37. R. Zang, Y. Xie, J. Liu, X. Meng, Y. Huang, and L. Wan: *J. Metall. Mater. Trans. A*, 2022, vol. 53, pp. 3210–5321.
38. J. Ruan and P H. J. China Machinery Industry Press, 1982, vol. 326.

39. Y. Yin, C. Du, Z. Zheng, T. Xie, K. Liu, and Y. Wu: *J. Chin. J. Nonferr. Met.*, 2006, vol. 16, pp. 1895–1901.
40. V.V. Gorskii, A.N. Gripachevskii, A.V. Vereshchak, B.M. Krivitskii, and V.A. Tsitovich: *J. Powder Metall. Met. C+*, 1993, vol. 32, pp. 308–13.
41. W.J. Zhang. Yangzhou University, 2019.
42. Su. Yunfeng, Y. Zhang, J. Song, and Hu. Litian: *J. Wear*, 2017, vol. 372–373, pp. 130–38.
43. N. Argibay, T.F. Babuska, J.F. Curry, M.T. Dugger, P. Lu, D.P. Adams, B.L. Nation, B.L. Doyle, M. Pham, A. Pimentel, C. Mowry, A.R. Hinkle, and M. Chandross: *J. Carbon*, 2018, vol. 138, pp. 61–68.
44. K.P. Furlan, D.E. Mello, and A.N. Klein: *J. Tribol. Int.*, 2018, vol. 120, pp. 280–98.
45. Y. Xian, Z. Zou, C. Tu, Y. Ding, T. Liao, F. Zhang, Q. Luo, G. Wu, and G. Gao: *J. Alloys Compd.*, 2020, vol. 835, p. 155444.
46. R.G. Chandrakanth, K. Rajkumar, and S.J. Aravindan: *Int. J. Adv. Manuf. Technol.*, 2010, vol. 48, pp. 645–53.
47. N. Tian, L.L. Dong, H.L. Wang, Y.Q. Fu, W.T. Huo, Y. Liu, J.S. Yu, and Y.S. Zhang: *J. Alloys Compd.*, 2021, vol. 867, p. 159093.
48. Y. Xiao, Z. Zhang, P. Yao, K. Fan, H. Zhou, T. Gong, L. Zhao, and M. Deng: *J. Tribol. Int.*, 2018, vol. 119, pp. 585–92.
49. C.-F. Han, H.-Y. Chu, R.-Y. Luo, N.-T. Liao, C.-C. Wei, G.-L. Chen, P.-H. Tsai, Y.-L. Chiu, Y.-C. Hwang, and J.-F. Lin: *J. Wear*, 2018, vol. 406–407, pp. 126–39.
50. S. Fan, L. Zhang, L. Cheng, G. Tian, and S. Yang: *J. Compos. Sci. Technol.*, 2010, vol. 70, pp. 959–65.
51. J. Zhang, Xu. Yongdong, L. Zhang, and L. Cheng: *Int. J. Appl. Ceram. Technol.*, 2007, vol. 4, pp. 463–69.
52. B. Lin, H. Wang, J. Wei, W. Zheng, Y. Ma, J. Wang, and T. Sui: *J. Ceram. Int.*, 2021, vol. 47, pp. 8627–33.
53. Y. Zhan and G. Zhang: *J. Mater. Des.*, 2006, vol. 27, pp. 79–84.
54. J.F. Archard: *J. Nature*, 1953, vol. 172, pp. 918–19.